Beat the diffraction limit in 3D direct laser writing in photosensitive glass

Matthieu Bellec[1,*], Arnaud Royon[1,3], Bruno Bousquet[1], Kevin Bourhis[2], Mona Treguer[2], Thierry Cardinal[2], Martin Richardson[3], and Lionel Canioni[1]

[1]*Centre de Physique Moléculaire Optique et Hertzienne, Université de Bordeaux, 351 cours de la Libération, 33405 Talence, France*

[2]*Institut de Chimie de la Matière Condensée de Bordeaux, Université de Bordeaux, 87 avenue du Docteur Schweitzer, 33608 Pessac, France*

[3]*College of Optics and Photonics/CREOL, University of Central Florida, 4000 Central Florida Boulevard, Orlando, Florida 32816, USA*

m.bellec@cpmoh.u-bordeaux1.fr

Abstract: Three-dimensional (3D) femtosecond laser direct structuring in transparent materials is widely used for photonic applications. However, the structure size is limited by the optical diffraction. Here we report on a direct laser writing technique that produces subwavelength nanostructures independently of the experimental limiting factors. We demonstrate 3D nanostructures of arbitrary patterns with feature sizes down to 80 nm, less than one tenth of the laser processing wavelength. Its ease of implementation for novel nanostructuring, with its accompanying high precision will open new opportunities for the fabrication of nanostructures for plasmonic and photonic devices and for applications in metamaterials.

©2009 Optical Society of America

OCIS codes: (160.5335) Photosensitive materials; (190.4720) Optical nonlinearities of condensed matter; (320.2250) Femtosecond phenomena; (350.3450) Laser-induced chemistry.

References and links

1. R. R. Gattass, and E. Mazur, "Femtosecond laser micromachining in transparent materials," Nat. Photonics **2**(4), 219–225 (2008).
2. K. Miura, J. Qiu, H. Inouye, T. Mitsuyu, and K. Hirao, "Photowritten optical waveguides in various glasses with ultrashort pulse laser," Appl. Phys. Lett. **71**(23), 3329–3331 (1997).
3. A. Zoubir, M. Richardson, L. Canioni, A. Brocas, and L. Sarger, "Optical properties of infrared femtosecond laser-modified fused silica and application to waveguide fabrication," J. Opt. Soc. Am. B **22**(10), 2138–2143 (2005).
4. E. N. Glezer, M. Milosavljevic, L. Huang, R. J. Finlay, T.-H. Her, J. P. Callan, and E. Mazur, "Three-dimensional optical storage inside transparent materials," Opt. Lett. **21**(24), 2023–2025 (1996).
5. L. Canioni, M. Bellec, A. Royon, B. Bousquet, and T. Cardinal, "Three-dimensional optical data storage using third-harmonic generation in silver zinc phosphate glass," Opt. Lett. **33**(4), 360–362 (2008).
6. S. Kawata, H. B. Sun, T. Tanaka, and K. Takada, "Finer features for functional microdevices," Nature **412**(6848), 697–698 (2001).
7. F. Huo, Z. Zheng, G. Zheng, L. R. Giam, H. Zhang, and C. A. Mirkin, "Polymer pen lithography," Science **321**(5896), 1658–1660 (2008).
8. A. Chimmalgi, C. P. Grigoropoulos, and K. Komvopoulos, "Surface nanostructuring by nano-/femtosecond laser-assisted scanning force microscopy," J. Appl. Phys. **97**(10), 104319 (2005).
9. S. G. Johnson, and J. D. Joannopoulos, "Three-dimensionally periodic dielectric layered structure with omnidirectional photonic band gap," Appl. Phys. Lett. **77**(22), 3490–3492 (2000).
10. M. S. Rill, C. Plet, M. Thiel, I. Staude, G. von Freymann, S. Linden, and M. Wegener, "Photonic metamaterials by direct laser writing and silver chemical vapour deposition," Nat. Mater. **7**(7), 543–546 (2008).
11. H. Schneckenburger, D. F. Regulla, and E. Unsöld, "Time-resolved investigations of radiophotoluminescence in metaphosphate glass dosimeters," Appl. Phys., A Mater. Sci. Process. **26**, 23–26 (1981).
12. A. V. Dmitryuk, S. E. Paramzina, A. S. Perminov, N. D. Solov'eva, and N. T. Timofeev, "The influence of glass composition on the properties of silver-doped radiophotoluminescent phosphate glasses," J. Non-Cryst. Solids **202**(1-2), 173–177 (1996).
13. I. Belharouak, C. Parent, B. Tanguy, G. Le Flem, and M. Couzy, "Silver aggregates in photoluminescent phosphate glasses of the 'Ag_2O-ZnO-P_2O_5' system," J. Non-Cryst. Solids **244**(2-3), 238–249 (1999).
14. H. D. Jones, and H. R. Reiss, "Intense-field effects in solids," Phys. Rev. B **16**(6), 2466–2473 (1977).

#110443 - $15.00 USD Received 22 Apr 2009; revised 25 May 2009; accepted 26 May 2009; published 4 Jun 2009

15. B. C. Stuart, M. D. Feit, S. Herman, A. M. Rubenchik, B. W. Shore, and M. D. Perry, "Nanosecond-to-femtosecond laser-induced breakdown in dielectrics," Phys. Rev. B **53**(4), 1749–1761 (1996).
16. L. V. Keldysh, "Ionization in the field of a strong electromagnetic wave," Sov. Phys. JETP **20**, 1307–1314 (1965).
17. C. B. Shaffer, J. F. Garcia, and E. Mazur, "Bulk heating of transparent materials using a high-repetition-rate femtosecond laser," Appl. Phys., A Mater. Sci. Process. **76**, 351–354 (2003).
18. S. M. Eaton, H. Zhang, P. R. Herman, F. Yoshino, L. Shah, J. Bovatsek, and A. I. Arai, "Heat accumulation effects in femtosecond laser-written waveguides with variable repetition rates," Opt. Express **13**(12), 4708–4716 (2005).
19. L. A. Pipes, and L. R. Harvill, "Applied mathematics for engineers and physicists" (McGraw-Hill International Edition, 1987).
20. Y. Dai, X. Hu, C. Wang, D. Chen, X. Jiang, C. Zhu, B. Yu, and J. Qiu, "Fluorescent Ag nanoclusters in glass induced by an infrared femtosecond laser," Chem. Phys. Lett. **439**(1-3), 81–84 (2007).
21. A. Podlipensky, V. Grebenev, G. Seifert, and H. Graener, "Ionization and photomodification of Ag nanoparticles in soda-lime glass by 150 fs laser irradiation: a luminescence study," J. Lumin. **109**, 135–142 (2004).
22. L. A. Peyser, A. E. Vinson, A. P. Bartko, and R. M. Dickson, "Photoactivated fluorescence from individual silver nanoclusters," Science **291**(5501), 103–106 (2001).
23. M. Treguer, F. Rocco, G. Lelong, A. Le Nestour, T. Cardinal, A. Maali, and B. Lounis, "Fluorescent silver oligomeric clusters and colloidal particles," Solid State Sci. **7**(7), 812–818 (2005).
24. T. Tani, "The theory of the photographic process" (Oxford University Press, New York, 1995).
25. S. Stookey, "Photosensitive Glass : A New Photographic Medium," Ind. Eng. Chem. **41**, 856–861 (1949).
26. G. Mie, "Contribution to the optics of turbid media, particularly of colloidal metal solutions," Ann. Phys. **25**, 377–445 (1908).
27. H. C. Van De Hulst, "Light scattering by small particles" (J. Wiley & Sons, 3rd edition, New York, 1964).
28. L. N. Gaier, M. Lein, M. I. Stockman, P. L. Knight, P. B. Corkum, M. Yu Ivanov, and G. L. Yudin, "Ultrafast multiphoton forest fires and fractals in clusters and dielectrics," J. Phys. B **37**(3), L57–L67 (2004).
29. O. M. Efimov, K. Gabel, S. V. Garnov, L. B. Glebov, S. Grantham, M. Richardson, and M. J. Soileau, "Color-center generation in silicate glasses exposed to infrared femtosecond pulses," J. Opt. Soc. Am. B **15**(1), 193–199 (1998).
30. J. Crank, "The mathematics of diffusion" (Clarendon Press, 1956).
31. W. T. Doyle, "Absorption of Light by Colloids in Alkali Halide Crystals," Phys. Rev. **111**(4), 1067–1072 (1958).

1. Introduction

3D femtosecond laser direct writing is used to modify the structure of transparent materials, such as glasses or polymers, for photonic applications [1]: waveguides [2,3], optical data storage [4,5] and localized polimerization [6]. Like any optical technique, the size of the interaction area is limited by the optical diffraction. The limiting factors are the processing laser wavelength and the numerical aperture of the focusing system. Thanks to nonlinear interaction at the focus of the laser beam, the size of the 3D photo-induced structures can be reduced but is still related to the limiting parameters. Up to now, with a UV laser and a high NA objective corresponding to a diffraction limit of 350 nm, using multiphoton absorption and threshold effects, structures of about 120 nm have been demonstrated in polymers [6].

Although much smaller feature sizes can be achieved with nanolithographic [7] or near field optical [8] techniques, they suffer from being limited to two dimensional geometries. With additional tooling costs, lithographic techniques can be extended to three dimensions using layer-on-layer approaches [9], and recently, a technique that combines direct laser writing and metal deposition permits to create nanostructures [10]. However all these techniques suffer from several drawbacks that include slow processing speeds, complexity in implementation and the availability of materials and patterns.

Here we present a new approach for direct laser writing by using a high repetition rate infrared femtosecond laser. Subwavelength nanostructures are created independently from the limiting factors. We apply this new method in a photosensitive glass containing silver. The nanostructures are formed by the writing process as a spatial distribution of silver species embedded in the glass matrix. Two types of silver species can be created, silver clusters that act as fluorescence emitters and silver nanoparticles which have plasmonic properties.

#110443 - $15.00 USD Received 22 Apr 2009; revised 25 May 2009; accepted 26 May 2009; published 4 Jun 2009
(C) 2009 OSA

2. Experimental details

2.A. Photosensitive glass preparation

The processed glass is highly photosensitive and was originally developed as a gamma irradiation dosimeter [11,12]. It is a zinc phosphate glass containing silver ions [13] presenting an ultraviolet (UV) absorption band below 280 nm. Following exposure to gamma rays, the glass presents a broad UV absorption band, and when excited by UV radiation, emits homogeneous fluorescence which intensity is proportional to the irradiation dosage. This fluorescence is attributed to the presence of silver clusters. In the experiments, these fluorescent silver clusters behave as probe for the laser/glass interaction.

Glasses with composition $40P_2O_5$-$4Ag_2O$-$55ZnO$-$1Ga_2O_3$ (mol%) were made using a standard melt quench technique. $(NH_4)2HPO_4$, ZnO, $AgNO_3$ and Ga_2O_3 in powder form were used as raw materials and placed with the appropriate amount in a platinum crucible. A heating rate of about 1°C.min^{-1} has been conducted up to 1000°C. The melt was then kept at this last temperature (1000°C) from 24 to 48 hours. Following this step, the liquid was poured into a brass mold after a short increase of the temperature at 1100°C in order to access the appropriate viscosity. The glass samples obtained were annealed at 320°C (55°C below the glass transition temperature) for 3 hours, cut (0.5 to 1 mm-thick) and optically polished. The glass possesses an absorption cut-off wavelength at 280 nm (due to the silver ions associated absorption band around 260 nm) and emits fluorescence mainly around 380 nm when excited at 260 nm. This intrinsic fluorescence is due to Ag^+ isolated in the glass.

2.B. Sample exposure

In the present experiments, nanostructures are created by a pulse train from a near infrared (NIR) femtosecond laser focused with a microscope objective inside the glass at an irradiance I below the refractive index modification threshold (I < 2.5 TW.cm^{-2}, corresponding to 1.2 J.cm^{-2}).

The glass sample was irradiated using a femtosecond laser oscillator source emitting 470 fs, 9.44 MHz repetition rate pulses at 1030 nm. The laser mode is TEM_{00}, M^2 = 1.2 and the output polarization is TM. The maximum output average power is close to 6 W, which results in a maximum energy per pulse of 600 nJ. Acousto-optic filtering permits the tuning of the pulse energy and the repetition rate for control of the cumulated effect. The femtosecond laser is focused using a reflective 36 × objective with a 0.52 NA (working distance 15 mm) at a depth of 200 µm in the glass. The beam waist is estimated to be 1 µm. The glass was exposed to different fluence levels, between 0.5 J.cm^{-2} to 1.5 J.cm^{-2}, and different numbers of pulses, from 10^2 to 10^6. In order to avoid glass damage, the laser fluence of 1 J.cm^{-2} was chosen in order to optimize the nanostructuring process. The sample was manipulated using a micro-precision xyz stage.

2.C. Sample analysis

A High Reflection Scanning Electron Microscope (HRSEM JEOL 6700F – gun field emission – resolution 1.1 nm) and Atomic Force Microscope (AFM D.I. 3100 Veeco AFM) were used for irradiated sample analysis. For HRSEM and AFM techniques, a topology modification is needed to obtain a contrasted image. When composed of silver clusters, the nanostructures present no topological changes. Thus, an acid treatment, 10 seconds in chloride acid, was performed on each sample to reveal the nanostructures. Acid etches preferentially the silver containing area. The fluorescence and absorption spectral measurements have been performed with a Triax 550 Jobin Yvon spectrometer associated to a home made confocal microscope. An excitation Hg lamp with appropriate filter set was used for fluorescence studies and De, halogen white lamp for absorption measurement.

#110443 - $15.00 USD Received 22 Apr 2009; revised 25 May 2009; accepted 26 May 2009; published 4 Jun 2009
(C) 2009 OSA

3. Results and analysis

3.A. Nanostructure formation

The components of this new direct writing process are illustrated in Fig. 1. Two principal physical phenomena with different time scales are involved in the nanostructuring process.

The first mechanism occurs on a short time scale commensurate with the laser pulse duration. Instantaneous with the laser pulse, a nonlinear multiphoton interaction occurs, in this case 4-photon-absorption, in which photoelectrons are ejected from the valence to the conduction band of the glass [14–16]. The photo-excitation process is detailed in the Appendix A. In a similar manner to the mechanism utilized in a dosimeter [11,12], the released electrons are trapped within a few picoseconds by silver Ag^+ ions to form silver Ag^0 atoms (blue spots in Fig. 1(A)). Since this is produced by a highly nonlinear interaction, the silver atoms are distributed in an area that is smaller than the laser beam diameter [6]. The blue circle in Fig. 1(A) denotes this area. This configuration defines the initial conditions for the mechanism.

The second physical process occurs on a longer timescale of a few microseconds. Due to the high laser repetition rate, the accumulation of the deposited laser energy increases the local temperature [17,18], see Appendix B.A. After several thousands of pulses, the diffusion of the initial distribution of silver species occurs. Ag^0 atoms are considered as the most mobile species. According to the Fick's laws, the Ag^0 diffusion follows the thermal and concentration gradients from the center to the edges of the pulse [19]. This migration is represented by the red arrows in Fig. 1(B). Mobile Ag^0 atoms are trapped by the Ag^+ ions to form silver clusters Ag_m^{x+} with the number of atoms $m<10$ and the ionization degree x (red spots in the Fig. 1(C)). As a consequence, the local Ag^+ ions density is progressively diminished [11,12]. The silver clusters are chemically more stable in the glass matrix as compared to the Ag^0 atoms and present an absorption band in the near UV range (320 nm-380 nm) corresponding to level positions within the band gap. Silver clusters formation leads to the interruption of the diffusion processes due to small mobility of Ag_m^{x+} in the glass. Subsequent laser pulses maintain the heating process in the glass and interact with the newly-created silver clusters. As illustrated in Fig. 1(C), the Ag_m^{x+} are photo-dissociated in the center of the laser beam. The photo-dissociation threshold is represented by the green circle in Fig. 1(C). As a result, a cylindrical structure composed of silver clusters is formed on the edges of the laser beam.

#110443 - $15.00 USD Received 22 Apr 2009; revised 25 May 2009; accepted 26 May 2009; published 4 Jun 2009
(C) 2009 OSA

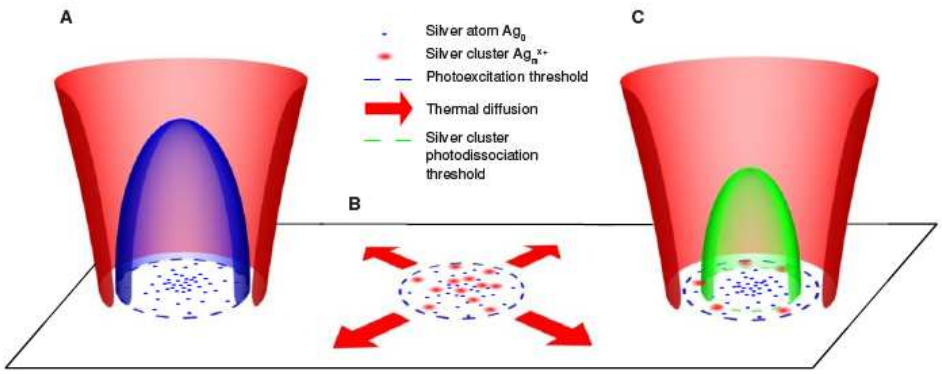

Fig. 1. Schematic view of the nanostructures formation. (A) Following laser irradiation, released photoelectrons are trapped by Ag^+ ions to form silver atoms Ag^0, represented by the blue spots. The Ag^0 distribution follows the interaction area delimited by the blue dashed circle. The area is smaller than the laser beam size because of the nature of the nonlinear interaction. (B) After 1000 pulses, the local temperature increases and the diffusion occurs, as illustrated by the red arrows. Ag^0 and Ag^+ interact to give rise to silver clusters Ag_m^{x+} with m<10, illustrated by the red spots. (C) Subsequent laser pulses photo-dissociate the newly formed Ag_m^{x+} except on the edges of the interaction area, leaving a cylindrical nanostructure composed of silver clusters. The silver cluster photo-dissociation threshold is represented by the green dotted circle.

Figure 2 presents the normalized spatial distribution of the local silver atoms calculated for different numbers of laser pulses. Typically, the concentration of Ag^0 is reduced by a factor of 10 after 10^5 pulses. We suppose that all the diffused Ag^0 are transformed to create silver clusters Ag_m^{x+} on the edges of the laser beam. In this calculation, the thickness of the structure is considered infinitely small because the very small diffusion coefficient and the photochemistry kinetics of the silver clusters are not taken into account. Details on the calculation are available in the Appendix B.B.

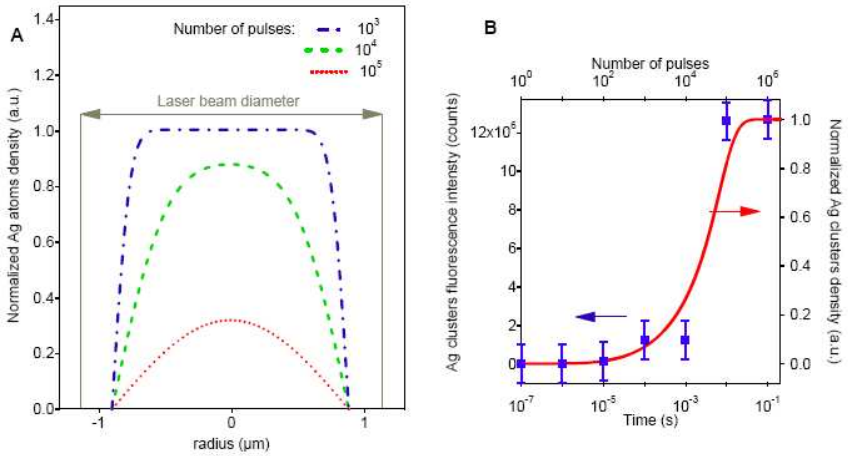

Fig. 2. Modeling of the silver species density. (A) The calculated Ag^0 density is represented in the center of the laser beam for different numbers of pulses (from 10^3 to 10^5). The Ag^0 atoms density decreases with the number of pulses because diffusion process brings them to the edges of the laser beam. In this simulation, it is an effective diffusion process which takes into account the photo-dissociation effect, see Appendix B.B. The boundary condition on the edges keeps the Ag^0 density to zero because they are consumed to form silver clusters. (B) The calculation of the corresponding created Ag_m^{x+} is represented and compared to the fluorescence measurements.

#110443 - $15.00 USD Received 22 Apr 2009; revised 25 May 2009; accepted 26 May 2009; published 4 Jun 2009
(C) 2009 OSA

3.B. Nanostructure observation

Experimentally, silver clusters are distributed with sizes much smaller than the diffraction limit. Figure 3(A) presents a high resolution scanning electron microscopy (HRSEM) image of a zone irradiated at 1 J.cm^{-2} with 10^6 pulses. After polishing to bring the nanostructure to the surface, the sample is acid-etched before imaging to enable the localization and the characterization of the nanostructures. As expected, an annular shape is observed. Figure 3(B) shows that the profile of the structure is only 80 nm wide. It is of great interest to note that HRSEM allows topological and chemical characterization. Atomic Force Microscopy (AFM) is a complementary measurement and allows topological characterization. A comparison between the transversal profiles of the HRSEM image (Fig. 3(C)) and the corresponding AFM image (Fig. 3(D)) shows that the contrasted signal from the annular shape is due to a chemical change induced by the accumulation of Ag species. The central peak indicates a topological modification. Indeed, the remaining silver concentration linked to the silver migration, modifies the glass composition. A selective acid-etching has occurred in the composition of the modified zones giving rise to topological changes.

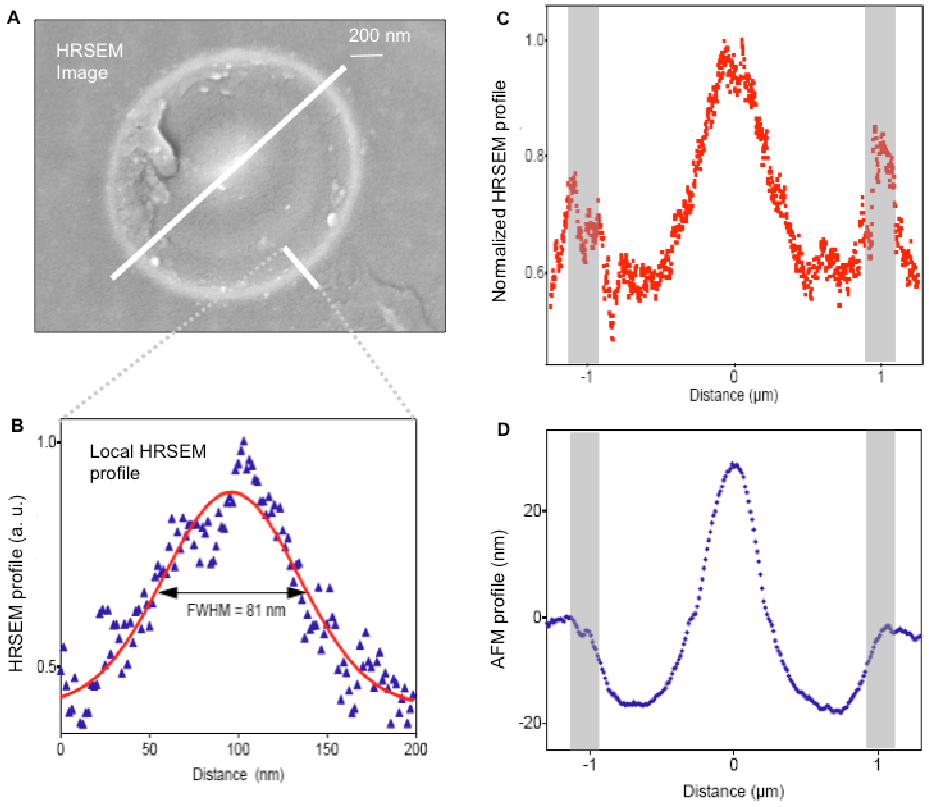

Fig. 3. HRSEM and AFM characterization of the nanostructures. The irradiated sample was acid-etched to reveal the nanostructures. HRSEM allows topological and chemical characterization. AFM allows topological characterization. (A) HRSEM image of a spot irradiated by a focused femtosecond laser at 1 J.cm^{-2}. As expected, a circular shape is observed. (B) The transversal profile (small white segment) of the HRSEM image has a measured width of ~80 nm (FWHM). (C) and (D) Comparison between the transversal profiles (following long white segment) of the HRSEM image (C) and the corresponding AFM image (D) shows that the annular shape is due to chemical modifications (accumulation of Ag species). The central peak indicates a topological modification following acid-etching.

#110443 - $15.00 USD Received 22 Apr 2009; revised 25 May 2009; accepted 26 May 2009; published 4 Jun 2009
(C) 2009 OSA

3.C. Creation of fluorescent silver clusters

The distribution of these clusters after laser irradiation can be visualized by confocal fluorescence microscopy. The silver clusters Ag_m^{x+} embedded in the zinc phosphate glass exhibit a strong fluorescence when they are excited in the UV-blue range (from 300 nm up to 500 nm) of the spectrum [20,21]. A 3D reconstruction of the laser induced structures is presented in Fig. 4(A). The fluorescent silver clusters are organized, on the edges of the interaction voxel defined by the nonlinear interaction, as a cigar shape with a diameter smaller than the laser beam one and with a length limited by the confocal parameter. Figure 4(B) shows the fluorescence emission spectrum for an excitation wavelength at 405 nm. A few studies have attributed the fluorescence to specific clusters in glass and show strong dependence with host matrix, ionization degree and cluster geometry. In our case, a band and a shoulder can be observed, one at 500 nm and another at 610 nm, which could be attributed to Ag_m^{x+} silver clusters [20–23]. In Fig. 2(B), the fluorescence signal obtained after laser irradiation for different numbers of pulses is compared to the calculated silver clusters density. Experimentally, we observed that more than 1000 pulses are needed to initiate the formation of silver clusters, corresponding to the thermal activation of silver Ag^0 diffusion. After 10^5 pulses, a saturation effect appears, due to the total diffusion of the induced Ag^0 atoms.

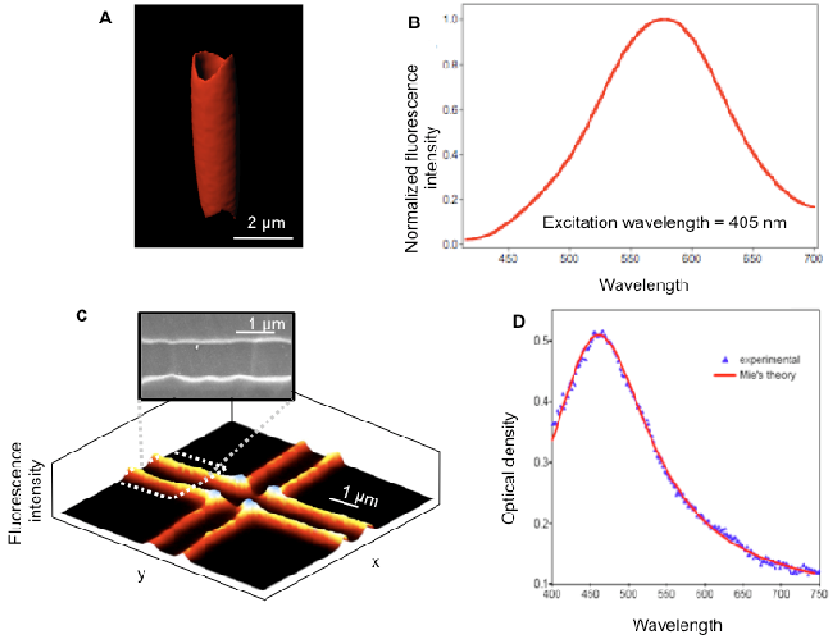

Fig. 4. Optical properties of silver nanostructures. The silver clusters exhibit strong fluorescence when excited in the UV-blue range. The silver nanoparticles reveal a surface plasmon resonance. (A) 3D reconstitution of confocal fluorescence microscopy images of a 1 $J.cm^{-2}$ laser irradiated spot. (B) Fluorescence spectrum of the photo-induced silver clusters with an excitation wavelength of 405 nm. A characteristic band centered at 580 nm is observed. (C) Fluorescence microscopy and corresponding HRSEM images of a cross pattern created by moving the sample first in the x direction and second in the y direction. During the second pass, the previously-created silver clusters are photo-dissociated. (D) Following laser irradiation, the sample is thermally treated at 400°C during 20 minutes to transform the silver clusters into silver nanoparticles. A differential absorbance spectrum is performed in the region where the nanostructures are formed (red dots). The band centered at 460 nm is characteristic of the surface plasmon resonance of the silver nanoparticles arrangement. The experimental measurement fitted with the Mie's theory gives a mean diameter of 10 nm (blue curve).

#110443 - $15.00 USD Received 22 Apr 2009; revised 25 May 2009; accepted 26 May 2009; published 4 Jun 2009
(C) 2009 OSA

In summary, the process of laser interaction in this glass can be viewed as a paintbrush and an eraser working together on the nanoscale. The paintbrush acts on the edges of the laser beam and the eraser works at the center. Arbitrary 3D patterns can be written in the photosensitive glass. As an example, Fig. 4(C) presents a cross pattern produced by moving the sample first in the x direction and then in the y direction at 1 $mm.s^{-1}$, corresponding to 10^4 $pulses.\mu m^{-1}$. The size of the structure measured by fluorescence confocal microscopy is limited by the resolution at 350 nm in our conditions. The insert in Fig. 4(C) presents a HRSEM image of the nanostructure. As expected, nanoscale lines containing silver clusters are written. The second pass crosses the center of the x line perpendicularly and clearly photo-dissociates the previously-created silver clusters. Moreover, the weaker fluorescence signal close to the y line indicates that the silver species in the center were only partially transformed.

For use in nanostructuring applications, the stability of the photo-induced silver clusters is investigated. First, annealing the exposed glass at temperatures from 100°C up to 300°C shows no dissociation of the clusters. Second, under UV light exposure for several hours, no change in the fluorescence spectrum nor in the clusters distribution are observed. These results indicate that the silver clusters are stably embedded in this zinc phosphate glass matrix. We have also performed the same experiments with a silver-doped silicate glass matrix. Similar nanostructures were created as described for the phosphate glass host, but the stability is reduced to a few hours under UV exposure.

3.D. Creation of silver nanoparticles

At this point, the nanostructure is composed of silver clusters and is, by analogy with silver photography [24], a latent image in that no visible change in the refractive index is evident. To obtain a contrasted image, these clusters need to be thermally developed to form silver nanoparticles [25]. Following laser irradiation, the glass sample is annealed at 400°C, which is 20°C below the glass transition temperature, for 20 minutes. The absorption spectrum in the annealed region is monitored until the wide band centered around 460 nm, which is characteristic of the surface plasmon resonance of nanoparticles, is observed (Fig. 4(D)). The well-known Mie's theory [26,27] for silver nanoparticles embedded in a glass matrix demonstrates that intensity, resonant position and bandwidth of the absorption spectrum depend on the size, the filling factor and surroundings of the silver nanoparticles. The Mie's model is used to fit the experimental data (blue curve in Fig. 4(D)), see Appendix B.C. A mean particle size of 10 nm is found.

4. Conclusion

This universal mechanism could be used for various ions doped matrixes (glass, polymer) in which reduction process and thermal diffusion are involved, thanks to the high repetition rate femtosecond laser. The 3D laser direct writing of various nanostructures (silver clusters, silver nanoparticles) can be extended in a number of ways. Various properties of the structures could be exploited in the photonics and plasmonics fields. As an example, the silver clusters exhibit strong nonlinearities without modifying the linear refractive index. Thus, efficient 3D optical data storage can be realized in the glass [5]. The silver clusters, distributed in an area below the diffraction limit, are local fluorescent emitters. Moreover, nanoparticles exhibit many properties, such as plasmon resonance absorption, local field enhancement, local refractive index modification, etc… Designing 3D nanostructures containing nanoparticles, with an ease of use, offers a new alternative for the fabrication of 3D photonics crystals, metamaterials and plasmonic devices.

Appendix A: Details on the photo-excitation process

Various photo-excitation processes occur and are in competition at the early stage of the laser/glass interaction: multiphoton [14], tunneling [16], avalanche [15], multiphoton "forest

#110443 - $15.00 USD Received 22 Apr 2009; revised 25 May 2009; accepted 26 May 2009; published 4 Jun 2009
(C) 2009 OSA

fires" [28] ionizations or combinations between spectral broadening and linear or two-photon absorption of the laser pulse [29]. In order to investigate the photo-ionization mechanisms at the picosecond time scale involved in our photosensitive glass exposed to a high-repetition rate femtosecond pulse train, a transient absorption pump-probe experiment was performed.

A typical temporal dynamic of the plasma-induced-absorption for a pump irradiance of 7.3 TW.cm^{-2} is shown in Fig. 5. No absorption is present after 1.8 ps. Nevertheless, the temporal resolution of our experiment does not permit to reveal details below 1 ps. The absorption offset, which is about 0.05% at 7.3 TW.cm^{-2}, is due to thermal cumulative effects appearing when a high repetition rate laser is used. The maximum absorption measured at zero delay as a function of the pump irradiance is given in Fig. 6.

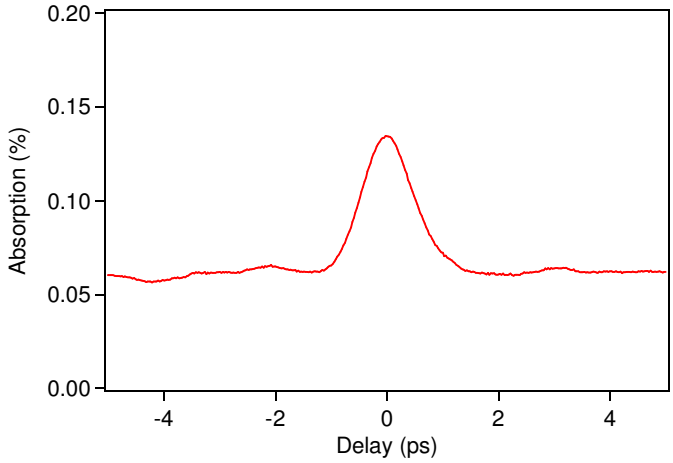

Fig. 5. Evolution of the plasma-induced-absorption versus the pump-probe delay for a pump irradiance of 7.3 TW.cm^{-2}. The curve is an average of 30 acquisitions. The standard deviation of these acquisitions gives an uncertainty of the measurement of 40%.

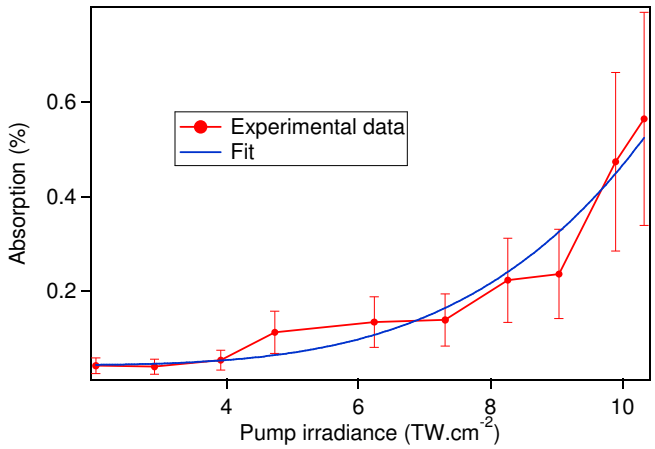

Fig. 6. Evolution of the plasma-induced-absorption versus the pump irradiance at the sample.

In a multiphoton absorption regime, the absorption should scale as $Abs(I) \propto I^k$, where k is the order of the multiphoton process and I the irradiance. A fit of the experimental data with a fixed value of k = 4 provides, with a good uncertainty, a clear evidence of four-photon absorption as the photo-ionization mechanism involved in the nanostructuring of our photosensitive glass.

#110443 - $15.00 USD Received 22 Apr 2009; revised 25 May 2009; accepted 26 May 2009; published 4 Jun 2009
(C) 2009 OSA

Assuming a simple Drude's model for the plasma, the free electron density N_e can be determined from the absorption measurements as follow:

$$N_e = \frac{cn_0\varepsilon_0 m_e}{e^2\tau_c L}\left(1+\frac{4\pi^2c^2\tau_c^2}{\lambda_0^2}\right)\ln\left(\frac{1}{T}\right) \quad (1)$$

where $n_0 = 1.58$ is the refractive index of the glass, $\tau_c = 0.4$ fs the electronic collision time, $L = 10$ µm the interaction length, λ_0 the laser wavelength and $T = 1$ - *Abs* the plasma-induced-transmission. We assume the interaction length is on the same order of magnitude than the confocal parameter $b = \frac{2\pi n w_0^2}{\lambda_0}$. The measured free electron density ranges from 0.2 to 3 × 10^{17} cm^{-3}, and is four orders of magnitude below the critical electron density, which is about 10^{21} cm^{-3} at the laser wavelength. In our glass, the Ag^+ ions density is about 3 × 10^{20} cm^{-3}. Assuming that each released electron is trapped by one Ag^+ ion, we can consider that 1 Ag^0 is formed per 1000 Ag^+ ions.

Appendix B: Calculations

B.A. Temperature evolution under laser irradiation

The laser used in our experiments presents a high repetition rate (9.44 MHz). Thus, the accumulation of the energy pulse after pulse in the glass leads to an increase of the temperature [17,18]. To represent the cumulative heating effects during the laser irradiation, we solve the 1D heat equation with a source term corresponding to the laser [30]:

$$\frac{\partial T(x,t)}{\partial t} - D_{th}\frac{\partial^2 T(x,t)}{\partial x^2} = \frac{Q(x,t)}{\rho C_p} \quad (2)$$

where T represents the temperature (K), D_{th} the thermal diffusion of the glass ($m^2.s^{-1}$), Q the heat source term ($J.s^{-1}.m^{-3}$), ρ the density of the glass ($kg.m^{-3}$) and C_p the specific heat capacity of the glass ($J.K^{-1}.kg^{-1}$).

The heat source term Q follows the laser temporal and spatial profiles and is defined as:

$$Q(x,t) = E_0 \exp\left(-\frac{Nx^2}{w_0^2}\right)\sum_{i=0}^{M}\delta\left(t-i\Delta t\right)H\left(t-i\Delta t\right) \quad (3)$$

with $E_0 = \frac{N^{3/2}\alpha E}{\pi^{3/2}w_0^2 w_z}$, α the absorption (%), E the pulse energy (J), N the number of photons absorbed during the interaction and w_0 and w_z the beam waist (m) and the Rayleigh length (m), respectively. M is the number of pulses and Δt the time interval between 2 pulses (s). δ is a temporal Dirac function (s^{-1}) assuming that the femtosecond pulse is infinitively short compared to the thermal timescale. H is an Heavyside function related to the causality principle.

By using the initial conditions, $T(t=0) = T(t=\infty) = T_0$, we can find an analytic solution:

#110443 - $15.00 USD Received 22 Apr 2009; revised 25 May 2009; accepted 26 May 2009; published 4 Jun 2009
(C) 2009 OSA

$$T(x,t)-T_0=\Delta T=\frac{\alpha EN}{2\pi^{3/2}w_0w_z\rho C_p}\sum_{i=0}^{M}\frac{\exp\left\{-\frac{x^2}{4\left[D_{th}\times(t-i\Delta t)+\frac{w_0^2}{4N}\right]}\right\}}{\left[D_{th}\times(t-i\Delta t)+\frac{w_0^2}{4N}\right]^{1/2}}H(t-i\Delta t) \quad (4)$$

ΔT depends on the glass and irradiation parameters summarized in Table 1.

Table 1. Experimental parameters for the temperature evolution calculation

Glass parameters		Laser parameters	
D_{th}	8 10^5 µm^2.s^{-1}	E	100 nJ
ρ	2.2 10^{-12} kg.µm^{-3}	$F = 1/\Delta t$	9.44 MHz
C_p	800 J.K^{-1}.kg^{-1}	w_0	1.07 µm
		w_z	5.44 µm

An important parameter is the deposited energy contributing to the temperature increase. This parameter is represented by α, the absorbed energy. We have first carried out a pulse to pulse absorption measurement to estimate the deposited energy per pulse. Figure 7 shows that less than 1% of the laser energy is absorbed by the glass. The transient absorption pump-probe experiment gives actually $\alpha = 0.04\%$.

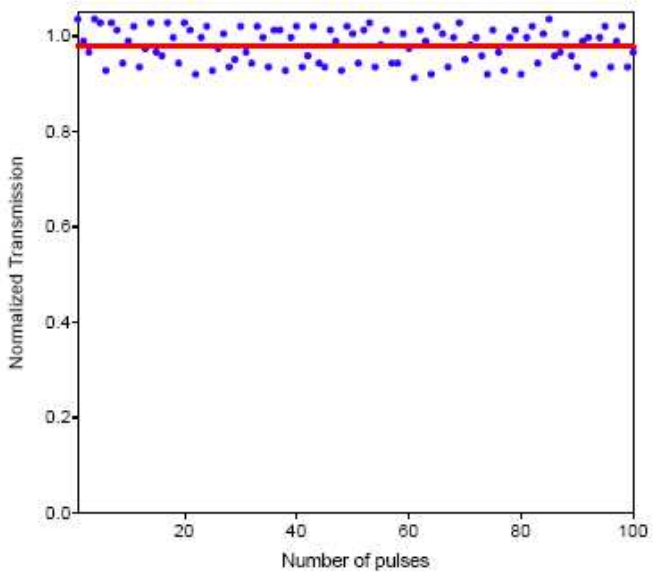

Fig. 7. Pulse to pulse transmission measurements (blue dot). The red line represents the mean value of the transmission which is less than 1%.

#110443 - $15.00 USD Received 22 Apr 2009; revised 25 May 2009; accepted 26 May 2009; published 4 Jun 2009
(C) 2009 OSA

The results of the calculation are presented in Fig. 8. To illustrate the cumulative effects, 2 regimes at 10 kHz and 10 MHz repetition rates, are compared in Fig. 8(A). In the 10 kHz regime (dotted blue curve), the temperature remains the same after several pulses. The temperature clearly increases in the 10 MHz regime (red curve). In this case, the time between two pulses is too short to allow the thermalization of the glass.

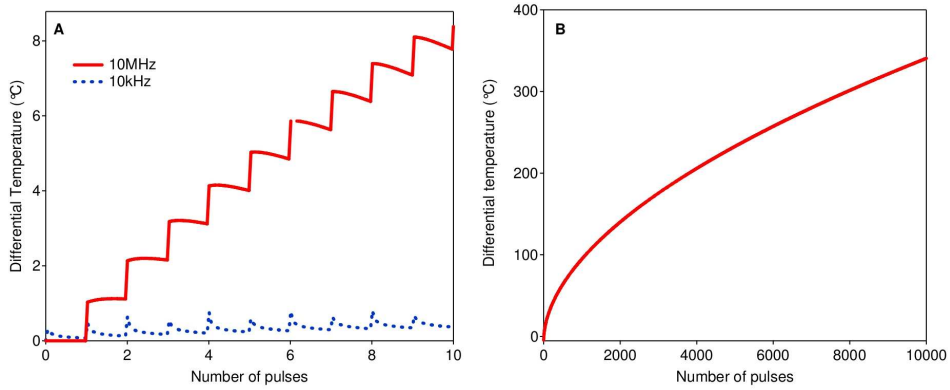

Fig. 8. Temperature versus the number of pulses. (A) The comparison between 10 kHz and 10 MHz repetition rate illustrates the cumulative effects of a high repetition rate laser. (B) Temperature elevation in our experimental condition. The thermal diffusion temperature (blue line) is achieved for 3000 pulses. The glass transition temperature is represented by the grey dotted line.

Figure 8(B) presents the results after several 1000 pulses in our experimental conditions. We can observe that the diffusion activation temperature for the silver (150 °C) is achieved after 2000 pulses. As represented by the grey dotted line, for 10000 pulses, the temperature is below the glass transition temperature (375°C). Thus, the maximal achieved temperature is sufficient to allow the diffusion of silver species but is too low to induce any strong damage in the glass.

B.B. Modeling of the diffusion mechanism

This calculation addresses on the diffusion and photo-dissociation effects of Ag^0 and silver clusters respectively, assuming that the electrons are created and trapped to form Ag^0 quasi-instantaneously compared to the diffusion time scale (µs). To simulate on a long time scale (µs) the silver cluster formation, different hypothesis was adopted. First, two regions can be distinguished. A central region where photo-dissociation of the silver clusters occurs and a periphery zone where the silver clusters can persist. Initially, the Ag^0 concentration which follows the laser deposited energy, presents a strong gradient. Then, assuming that following their formation, the silver clusters Ag_m^{x+} are immediately dissociated into Ag^0 atoms and Ag^+ ions, an effective Ag^0 diffusion in the central region can be considered. Moreover, assuming that the silver clusters have a very low mobility in the glass matrix and that the chemical reaction between Ag^0 and Ag^+ to form clusters is quasi-instantaneous, we can consider that the Ag^0 concentration drops to zero in the periphery zone. In this simplified model, the initial and boundary conditions for the Ag^0 diffusion equation were the existence of a strong Ag^0 concentration in the central region and no Ag^0 atoms on the periphery. An analytical solution was found in the 1D case, assuming that the silver cluster density corresponds to the integral difference between the initial and final (remaining) Ag^0 concentrations.

When the diffusion is activated, the initial distribution of Ag^0 is described by the Fick's laws summarized in the diffusion equation (Eq. (5)):

$$\frac{\partial N(x,t)}{\partial t} - D_{Ag}\frac{\partial^2 N(x,t)}{\partial x^2} = 0 \qquad \textbf{(5)}$$

#110443 - $15.00 USD Received 22 Apr 2009; revised 25 May 2009; accepted 26 May 2009; published 4 Jun 2009
(C) 2009 OSA

where N is the Ag^0 atoms density and D_{Ag} the silver diffusion coefficient ($m^2.s^{-1}$).

The initial and boundary conditions for the Ag^0 diffusion equation were chosen as follow: a strong Ag^0 concentration in the central region and a null Ag^0 concentration at the periphery, respectively. The initial density follows the spatial laser irradiance and is defined as:

$$N(x,t=0) = N_0 \exp\left(-\frac{kx^2}{w_0^2}\right) \tag{6}$$

where N_0 is the normalized Ag^0 density and can be estimated from the free electron density measurement.

For the 1D problem, we assume that $N_0 = 10^{20}$ cm^{-3}. k is the multiphoton absorption coefficient ($k = 4$) and w_0 is the beam waist. Due to the silver clusters creation at the edges of the laser beam, the boundary conditions are:

$$N(x=0,t>0) = N(x=a,t>0) = 0 \tag{7}$$

a corresponds to the length where the clusters are created. We take $a = w_0$.

An analytic solution is found in the 1D case. The diffusion of the Ag^0 is visualized for $x = \pm a$. Figure 2 of the paper represents the evolution of the Ag^0 density versus the time (*i.e.* the number of pulses). For $x = \pm a$, the silver clusters Ag_m^{x+} are formed and we consider that each Ag^0 participates to the formation of the Ag_m^{x+}. Thus, the Ag_m^{x+} density is defined as the difference between the initial Ag^0 density and the remainder Ag^0 density giving rise to the red curve in Fig. 4(C).

Here, we have considered that Ag^0 is the most mobile silver specie in the glass. Indeed, when reduced, silver species are not submitted to the electrostatics barriers and diffuse like particles in a viscous medium. By considering the diffusion coefficient ratio between Ag^+ and Ag^0 in the photographic process, we can assume that the diffusion coefficient of silver atom Ag^0 in the glass is larger than the silver ion Ag^+ one (1 $\mu m^2.s^{-1}$). The best fit of the fluorescence measurements (Fig. 4(C)) is found for $D_{Ag} = 50$ $\mu m^2.s^{-1}$.

B.C. Surface plasmon resonance calculation

The spectrum of an irradiated and heat-treated sample (Fig. 5) presents an absorption band characteristic of the silver nanoparticles. The evolution of the light scattering by small particles is well described by the Mie's theory [26,27]. According to this model, the absorption coefficient of small particles (with a radius R) at a wavelength λ_0 in a medium can be approximated as:

$$\alpha(\lambda_0) = \frac{24\pi^2 n_0^3 VN}{\lambda_0} \frac{\varepsilon_{r2}}{\left(\varepsilon_{r1} + 2n_0^2\right)^2 + \varepsilon_{r2}^2} \ (m^{-1}) \tag{8}$$

N is the number of nanoparticles per unit volume and V the mean volume of the nanoparticles. n_0 is the effective refractive index of the glass matrix. ε_{r1} and ε_{r2} are the real and imaginary part of the relative dielectric function of the silver particles ε_D defined using the Drude's model as:

$$\varepsilon_{rD}(\omega) = \varepsilon_{r1} + i\varepsilon_{r2} = 1 - \frac{\omega_p^2}{\omega^2 + i\Gamma\omega} \ \text{(unitless)} \tag{9}$$

where $\omega = 2\pi c/\lambda_0$ is the angular frequency, Γ the effective damping parameter for the free electron in the bulk silver metal. ω_p is the plasma angular frequency, defined as:

#110443 - $15.00 USD Received 22 Apr 2009; revised 25 May 2009; accepted 26 May 2009; published 4 Jun 2009
(C) 2009 OSA

$$\omega_p = \sqrt{\frac{N_e e^2}{\varepsilon_0 m_e}} \ (\text{rad.s}^{-1}) \tag{10}$$

where N_e and m_e are the density and the mass of the free charges, respectively. Considering that the mean radius of the nanoparticles is smaller than the electron mean free path, we can use the Doyle's formula and write the size dependence for the damping parameter [31]:

$$\Gamma_D(R) \sim \frac{V_f}{R} \ (\text{rad.s}^{-1}) \tag{11}$$

where V_f is the Fermi velocity of the electrons in bulk silver ($V_f = 1.39 \times 10^6$ m.s^{-1} in the case of silver).

Experimentally, we measure the evolution of the optical density versus the wavelength given theoretically by:

$$D(\lambda_0) = \frac{0.43 l \gamma}{NV} \alpha(\lambda_0) = \frac{A\lambda_0^2}{\left(\lambda_0^2 - \lambda_m^2\right)^2 + \frac{A}{D_m}\lambda_0^2} \ (\text{unitless}) \tag{12}$$

where γ is the volume concentration of nanoparticles (unitless) and l the thickness of the sample.

Using (Eq. (8) and (Eq. (9), we find:

$$A = \frac{0.43\left(48\pi^3 \varepsilon_0 n_0^3 c l \gamma m_e V_f\right)}{N_e e^2 R} \ (\text{m}^2) \tag{13}$$

The optical density presents a maximum value D_m at the wavelength λ_m defined by the resonant condition in (Eq. (8), $\varepsilon_{r1}(\omega_m) = -2n_0^2(\omega_m)$, with $\omega_m = 2\pi c/\lambda_m$. This gives:

$$D_m = \frac{0.43(24\pi^2 n_0^3 l\gamma)}{(1+2n_0^2)} \frac{1}{\Delta\lambda} \ (\text{unitless}) \tag{14}$$

$$\lambda_m^2 = \frac{4\pi^2 \varepsilon_0 c^2 m_e}{N_e e^2}(1+2n_0^2) \ (\text{m}^2) \tag{15}$$

where $\Delta\lambda$ is the Full Width at Half Maximum (FWHM) and is inversely proportional to R:

$$\Delta\lambda = \frac{\lambda_m^2 V_f}{2\pi c R} \ (\text{m}) \tag{16}$$

By fitting the experimental absorption curve, we found an average radius of the nanoparticles of 10 nm and a volume concentration of about 10^{-4}. The distribution of the nanoparticles at the edges of the laser beam is not taking into account for the calculation of the volume concentration. Locally, the nanoparticles are more concentrated. Moreover, we can note that the position of the resonance is red-shifted compared to the classical resonance for silver nanoparticles (420 nm) but, the intensity, the resonance position and the bandwidth of the absorption spectrum depends on other parameters. For example, the size distribution of the nanoparticles and the quantum size effects influence the bandwidth. The position of the resonance depends on the non-spherical shape and surrounding medium (refractive index, chemical interaction …).

#110443 - $15.00 USD Received 22 Apr 2009; revised 25 May 2009; accepted 26 May 2009; published 4 Jun 2009
(C) 2009 OSA

Acknowledgements

The authors acknowledge Sonia Gomez and the CREMEM platform (ICMCB-CNRS-University of Bordeaux) for the HRSEM images, Christine Labrugère and the CECAMA (ICMCB-CNRS-University of Bordeaux) for the AFM measurements, and Philippe Legros, Christel Poujol and the PICIN platform (Neurosciences Institute of the University of Bordeaux) for the confocal fluorescence microscopy. This work has been supported by the Agence Nationale de la Recherche (grant ANR-05-BLAN-0212-01), the CNRS (PICS grant 3179), the Aquitaine Region, the GIS AMA, the NSF and a FACE grant from the French Embassy in the US.

#110443 - $15.00 USD Received 22 Apr 2009; revised 25 May 2009; accepted 26 May 2009; published 4 Jun 2009
(C) 2009 OSA